ACS Macro Letters

Letter

pubs.acs.org/macroletters

Untying Knotted DNA with Elongational Flows

C. Benjamin Renner and Patrick S. Doyle*

Department of Chemical Engineering, Massachusetts Institute of Technology, Cambridge, Massachusetts 02139, United States

Supporting Information

ABSTRACT: We present Brownian dynamics simulations of initially knotted double-stranded DNA molecules untying in elongational flows. We show that the motions of the knots are governed by a diffusion−convection equation by deriving scalings that collapse the simulation data. When being convected, all knots displace nonaffinely, and their rates of translation along the chain are topologically dictated. We discover that torus knots "corkscrew" when driven by flow, whereas nontorus knots do not. We show that a simple mechanism can explain a coupling between this rotation and the translation of a knot, explaining observed differences in knot translation rates. These types of knots are encountered in nanoscale manipulation of DNA, occur in biology at multiple length scales (DNA to umbilical cords), and are ubiquitous in daily life (e.g., hair). These results may have a broad impact on manipulations of such knots via flows, with applications to genomic sequencing and polymer processing.

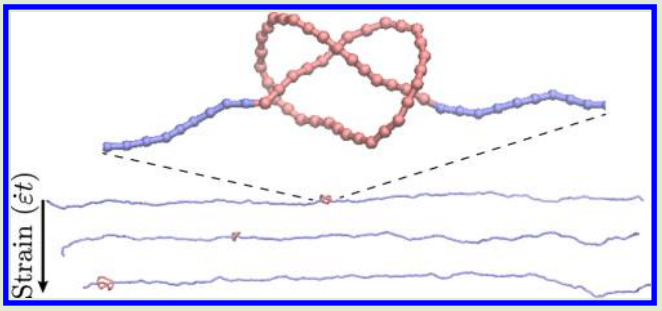

Knots are commonly encountered and manipulated in everyday experiences such as tying one's shoelaces or untangling spontaneously knotted strings.[1] Formally defined only for closed rings, the topologies of "open" knots (referred to hereafter simply as knots) are often unambiguous (e.g., shoelaces and neckties) and can be closed and algorithmically defined.[2−4] At microscopic scales, chromosomal knots are modified by topoisomerases during cell division[5] and are thought to participate in gene regulation.[6] Knots are found in proteins[7,8] and viral capsid DNA,[9,10] likely with yet to be fully understood functions. It has been mathematically proven that knots become asymptotically likely as the length of a polymer increases,[11] a fact that explains their ubiquity.

Due to the emerging significance of knotted polymers, a growing body of simulation literature is devoted to their study.[12,13] For instance, while the topology of a ring is fixed, an open polymer can spontaneously form and untie knots.[14] The probability of forming such knots can be nonmonotonic when the polymer is confined in slits[15,16] or tubes,[17] and increasing the stiffness of a polymer can similarly influence the knotting probability in unintuitive ways.[18,19] Such knots can substantially affect the mechanical properties[20,21] and rheological behavior[22] of a polymer, and the probability of forming knots has been used to infer the effective diameter of DNA molecules.[23] Recently, simulations have shown dramatic slowing of processes wherein a knot is *driven* along a chain such as entropic ejection of DNA from a viral capsid[24] and the translocation of single-stranded DNA (ssDNA)[25] and polypeptides[26] through pores.

Common nanofluidic experiments have led to the spontaneous formation of knots in DNA by collision with channel defects[27] or the application of moderate electric fields[28,29] during electrophoresis. More broadly, the growing library of methods to manipulate DNA molecules in nanofluidic devices has enabled fundamental research about single polymer molecules.[30,31] These studies inform important applications such as genomic sequencing via nanopore translocation[32] or direct linear analysis.[33] Thus, (un)tying knots in polymers is of interest in its own right. To this end, knots have been intentionally tied with optical tweezers in actin filaments[21] and double-stranded DNA (dsDNA).[34] Impressively, simulations reproduced the sizes and diffusion coefficients of dsDNA knots within a factor of 2.[35]

In this Letter, we use simulations to investigate the transport of a knot on a dsDNA molecule that has been extended by an elongational flow. We show that such flows cause the knot to be driven off the chain and untied, and we elucidate the relevant length and time scales for this process by examining the diffusion−convection equation. We observe that knots of different topologies translocate at different rates when strongly driven by the external flow. We show the different rates of knot translations are explained by a rotational mode of motion, available to torus knots,[36] that facilitates the translation of the knot, providing unique mechanistic insight.

We have used a Brownian dynamics approach to simulate dsDNA, which has been extensively parametrized by others.[35,37,38] The dsDNA molecule is represented by a fine-grained bead−spring model with $n_p = 5$ stiff bonds per persistence length, $l_p = 50$ nm. Screened Debye−Hückel interactions are used to model the long-range electrostatics of DNA−DNA interactions, and all simulations used an ionic strength of $I = 10$ mM, leading to a Debye length $\kappa^{-1} \approx 3$ nm

Received: August 4, 2014
Accepted: September 4, 2014

   dx.doi.org/10.1021/mz500464p | ACS Macro Lett. 2014, 3, 963−967

and a effective chain diameter of $w \approx 16$ nm.[23,39,40] These values were chosen to be representative of common low-salt conditions in microfluidic dsDNA experiments. An external planar elongational flow of the form $\mathbf{u}(\mathbf{r}_i) = \dot{\epsilon}(\hat{\mathbf{x}} - \hat{\mathbf{y}})\cdot\mathbf{r}_i$ was considered, where $\dot{\epsilon}$ is the strain rate and $\mathbf{r}_i$ is the position of the ith bead. We neglected interbead hydrodynamic interactions in this work, so the drag force on the ith bead is simply $\mathbf{F}_i^{\mathrm{d}} = \zeta_b[\mathbf{u}(\mathbf{r}_i) - (d\mathbf{r}_i/dt)]$ where ζ_b is the drag coefficient of a single bead. The Weissenberg number, $\mathrm{Wi} = \dot{\epsilon}\lambda$, is the appropriate dimensionless group for such flows. The DNA longest relaxation time, λ, was determined by fitting the long-time decay of the squared end-to-end distance of an initially stretched chain to a single exponential. See the Supporting Information (SI) for additional simulation details, including considerations of how the addition of intrabead hydrodynamic interactions and DNA torsional rigidity could alter the results of the simulations.

In Figure 1a, a snapshot of the 3_1 knot (Alexander–Briggs notation) on an extended DNA molecule at flow strength Wi = 16 is shown. The "knotted" region, identified algorithmically (see SI), is shown in red and the unknotted region in blue. The knot, initially centered in the internal chain coordinates, is ultimately driven to the end of the chain where it unties, shown in the snapshots in Figure 1b.

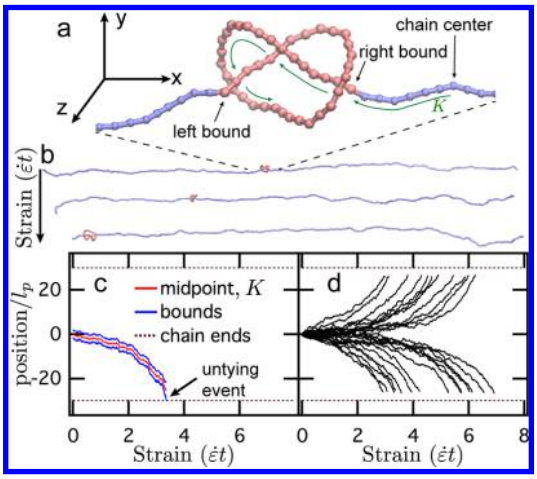

Figure 1. (a) Knotted (red) and unknotted (blue) regions of DNA extended by elongational flow (Wi = 16) for the 3_1 knot. The distance along the contour to the midpoint of the knot, K, is shown in green. (b) Simulation snapshots of an initially centered 3_1 knot untying from DNA at flow strength Wi = 16. (c) The midpoint and bounds of the knot pictured in (b) are plotted versus strain. (d) Untying trajectories of 25 initially centered 3_1 knots at flow strength Wi = 16.

Following previous studies,[41] the position of a knot is tracked in an "internal" chain coordinate by measuring the length of chain contour between the central index of the chain and the midpoint index of the knot, a length we denote as K. This scalar is signed: a negative sign indicates a position nearer the first index of the chain than the last, a positive sign the converse. The trajectory corresponding to the snapshots in Figure 1b is plotted in Figure 1c. A knot is considered to have "untied" itself when its boundary reaches the first or last index of the chain. The escape trajectories of 25 initially centered 3_1 knots are shown in Figure 1d. Knots escape to the left and right with equal probability, yet after moving a finite distance from the center, the directionality of escape is fixed. Furthermore, it is *extremely* difficult for a molecule that is extended by such a flow to form new knots. Thus, these results show the ability to guide the topology of a polymer to an unknotted state, which may be useful in the aforementioned applications.

We next explore the physics behind these observations. In a statistical sense, the evolution of knot trajectories corresponds to the evolution of an underlying probability density function, Ψ, of knot positions. This idea can be cast in the form of a diffusion–convection equation for a knot

$$\frac{\partial\Psi}{\partial t} = \nabla\cdot(D\nabla\Psi) - \nabla\cdot(\mathrm{u}\Psi) \tag{1}$$

where D is the diffusivity of the knot.

We consider the 1-D case of a knot with constant diffusivity confined to the stretching direction of the applied elongational flow, $\mathrm{u}_x = \dot{\epsilon}x$. We propose this scenario is the simplest approximation of the knot motion along a chain extended by an elongational flow (see SI). For this simplified system, the diffusion–convection equation becomes

$$\frac{\partial\Psi}{\partial t} = D\nabla^2\Psi - \dot{\epsilon}\left(x\frac{\partial\Psi}{\partial x} - \Psi\right) \tag{2}$$

Examination of eq 2 reveals the fundamental scale for time to be $\dot{\epsilon}^{-1}$. A length scale, $l = (D\dot{\epsilon}^{-1})^{1/2}$, emerges where the probability flux contributions due to diffusion and flow are balanced. To the first order, the motion of the knot will be diffusive for $|x| \ll l$ and follow the deterministic path of the flow for $|x| \gg l$. We independently measured knot diffusivities from chains held at the ends by constant tension (see SI). We found the diffusivity of the knots in this study to be topologically dependent but not strongly influenced by tension (and thus, Wi; see SI). Thus, the scalings depend on knot topology alone.

We simulated the process of a knot, initially centered in the internal chain coordinates ($K(t = 0) = 0$), escaping from a chain extended by elongational flow for a variety of topologies and flow strengths. In Figure 2a, the mean squared displacements of knot position are plotted versus time. The scalings from the

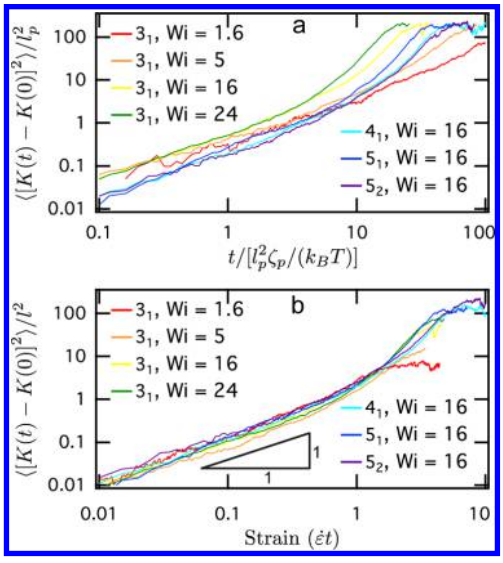

Figure 2. Mean squared displacements of initially centered knots ($K(t = 0) = 0$) in elongational flows. (a) Knot displacement plotted versus dimensionless time ($\zeta_p = n_p\zeta_b$). (b) Scaled knot displacement plotted versus strain. The triangle represents the slope of the diffusion-dominated mean squared displacement.

dx.doi.org/10.1021/mz500464p | ACS Macro Lett. 2014, 3, 963–967

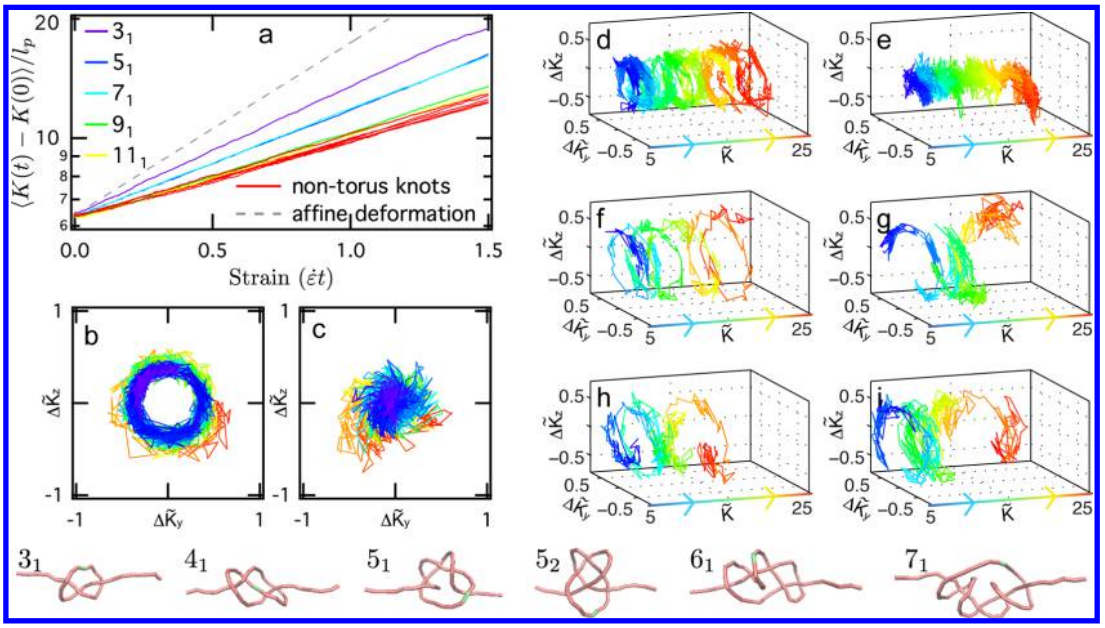

Figure 3. (a) Average knot displacements are plotted vs strain for various knots at flow strength Wi = 16 for knots initialized off-center ($K(t = 0) = 6l_p \gg l$ for all topologies). The nontorus knots consist of the following: 4_1, 5_2, 6_1, 6_3, 10_{28}, and 15n165258.[42] Displacements from the knot center of mass of the central segment of the knot made dimensionless by l_p ($\Delta\tilde{K}_y$ and $\Delta\tilde{K}_z$) for the 3_1 (b) and 4_1 (c) knots in the plane orthogonal to the extensional axis; color changes from blue to red as the knot moves off the chain. Displacements from the knot center of mass of the central segment of the knot ($\Delta\tilde{K}_y$ and $\Delta\tilde{K}_z$) in the plane orthogonal to the extensional axis plotted versus knot position ($\tilde{K} = K/l_p$) for the 3_1 (d), 4_1 (e), 5_1 (f), 5_2 (g), 7_1 (h), and 6_1 (i) knots. Color changes from blue to red as the knot moves off the chain. Bottom: snapshots of knots in (d–i) with central segments highlighted in green.

diffusion–convection equation, $\dot{\varepsilon}^{-1}$ for time and $l^2 = D\dot{\varepsilon}^{-1}$ for length, are used to rescale the data, plotted in Figure 2b. The collapse of the data is good, especially given the simplistic approximations implicit in the scalings. When $K/l \ll 1$, a slope of 1 agrees with the collapsed simulation averages, indicating a diffusion-dominated regime. When $K/l \gg 1$, the trajectories expectedly diverge from this slope, indicating the predicted dominance of the external flow, a convection-dominated regime. These results show an uncomplicated model can capture the dynamics of simple knots on chains in elongational flows. Furthermore, these results elucidate the fundamental length and time scales of interest in a practical application—untying knotted molecules with an elongational flow.

We next explore the convection-dominated regime, i.e., $K \gg l$, in greater detail for the following topologies: 3_1, 4_1, 5_1, 5_2, 6_1, 6_3, 7_1, 9_1, 10_{28}, 11_1, and 15n165258.[42] The mean displacements of these knots are plotted in Figure 3a. The slope of any given trajectory is less than that of affine deformation, indicating that all knots lag the applied flow. The degree to which they lag the flow, remarkably, is strongly influenced by topological class rather than size or self-diffusion coefficient. For instance, the 4_1 knot, despite being the second simplest knot, moves much slower than the larger 7_1 knot. The nontorus knots have remarkably similar rates of convection despite drastically different sizes and topologies. Moreover, the $(2n + 1)_1$ knots, all torus knots, convect faster than every other knot studied. As the crossing number of the torus knots increases, the mean displacements seem to asymptotically approach that of the nontorus knots.

These findings indicate the torus knots access an additional collective mode of motion while being driven along the chain. This idea is akin to topologically controlled breathing modes that have been described in knots under tension[43] but is distinct in that we propose driving the knot along the chain preferentially activates this dominant mode. To visualize the relative motion of knot segments, we examined the displacements of the knot midpoint from the knot center of mass in two axes orthogonal to the stretching direction, ΔK_y and ΔK_z, where $\Delta K_y = (\mathbf{r}_{(R+L)/2} - (1/(R - L + 1))\sum_{i=L}^{R}\mathbf{r}_i)\cdot\hat{\mathbf{y}}$ and L and R denote the indices of the left and right bounds of the knot. The projections of dimensionless versions of these quantities, $\Delta\tilde{K}_y = \Delta K_y/l_p$ and $\Delta\tilde{K}_z = \Delta K_z/l_p$, are plotted for the 3_1 and 4_1 knots in Figure 3b and c, respectively. The central segment of the 3_1 knot follows a circular trajectory around the center of mass of the knot, but the 4_1 knot shows no discernible pattern. The rotational modes of motion become evident in the plots in Figures 3(d–i). The 3_1, 5_1, and 7_1 knots demonstrate sustained "corkscrew" rotations of the central segment where, as the knot is driven down the chain by the elongational flow, a secondary global rotation of the knot develops. These sustained rotations are clearly specific to the knot, not the flow; the flow, itself, is irrotational. These trajectories sharply contrast to those of the 4_1 knot where no sustained rotation of the central segment can be seen. The 5_2 and 6_1 knots demonstrate half rotations of the central segment, but full rotations are absent. It is here that we make a critical mechanistic observation: all knots move via self-reptation of segments, yet the torus knot topologies permit that a global, sustained *rotation* of the knot facilitates an additional *translation* of that knot down the chain. The nontorus knots cannot access these means of transport due to topological self-interference (see SI for videos).

We tested this mechanistic insight by predicting the chirality of knot rotations from simplistic sketches for the 3_1 knot. The 3_1 knot exists in right- and left-handed chiralities. The sketches in Figure 4 show that for a knot of given chirality globally rotating the knot will produce a translational motion of the knot along the extended chain. Conversely, when a 3_1 knot of given chirality is being convected by an elongational flow, the

dx.doi.org/10.1021/mz500464p | ACS Macro Lett. 2014, 3, 963–967

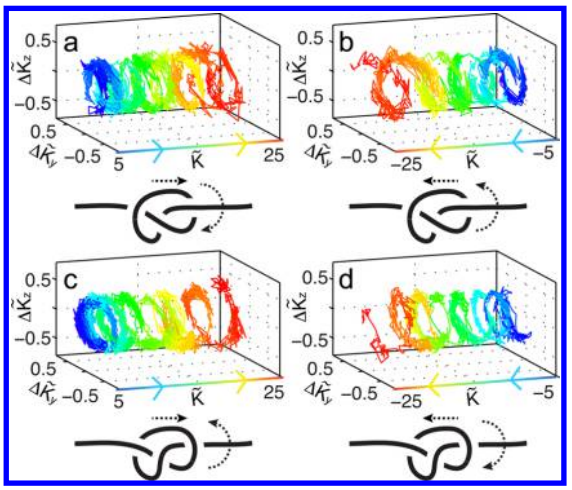

Figure 4. Displacements from the knot center of mass of the central segment of the knot ($\Delta\tilde{K}_y$ and $\Delta\tilde{K}_z$) in the plane orthogonal to the extensional axis plotted versus knot position ($\tilde{K}$) for the 3_1 knot. Color changes from blue to red as the knot moves off the chain. The right-handed (a and b) and left-handed 3_1 knots (c and d) rotate with opposite chiralities as they move off the right (a and c) and left (b and d) of the chain. All knots were initialized $K(t = 0) = \pm 6l_p$, $6l_p \gg l$ with flow strength Wi = 16.

chirality of rotation that coincides with the direction of translation can be predicted from the sketches. The colored trajectories in Figure 4 show the displacements of the central segments from the center of mass of knots of given chirality (right- or left-handed) being convected by an elongational flow off the right or left of the chain. The mechanism in the sketches is in complete agreement with the visualized simulation results. We have found this agreement between knot chirality, direction of knot translation, and knot rotation to hold in all observed simulation trajectories (~50); i.e., knot rotation always occurs as predicted by the sketches. These results confirm our idea that the translational motion of torus knots is facilitated by knot rotation. Further, this mechanism clearly extends to all of the $(2n + 1)_1$ family of torus knots; the addition of additional loops in the knot does nothing to prohibit the coupling of knot rotation and translation. The increased mobility of torus knots appears to be quite general, having been demonstrated in macroscopic shaking chain experiments,[44] simulations of DNA ejection from viral capsids,[45] and simulations of tensioned electrophoresing DNA.[46] We postulate our mechanism plausibly explains these results.

We have demonstrated the ability of elongational flows to untie knotted dsDNA molecules with computer simulations. Through scaling analysis, we revealed a critical length scale along the molecule that separates diffusive from convective transport of a knot in these flows. We have shown that a subset of knots, torus knots, can move linearly via sustained global rotation, which increases the speed at which they release from the chain. This represents an important mechanistic insight into the motion of driven knots, and since the mechanism is solely a function of topology, we expect it will apply in many other driven processes (e.g., nanopore sequencing or viral ejection of DNA) and for other polymers. We speculate that for longer DNA or for higher flow strengths self-jamming of knots may be observed as has been seen in tensioned knots,[26] and we hope future work will address this notion. Simulations show knots can jam nanopore translocation,[25] and experiments suggest jamming of knots during ultrafiltration of plasmid DNA.[47] Practically, our results could guide development of microfluidic devices that precondition molecules to unknotted states for such applications. Finally, since the model employed is parametrized to dsDNA at experimentally realizable conditions, we hope future experiments will test our results.

■ ASSOCIATED CONTENT

Supporting Information

Simulation details, knot identification procedures, knot diffusivities, simplification of the diffusion convection equation, and movies. This material is available free of charge via the Internet at http://pubs.acs.org.

■ AUTHOR INFORMATION

Corresponding Author

*E-mail: pdoyle@mit.edu.

Notes

The authors declare no competing financial interest.

■ ACKNOWLEDGMENTS

This work is supported by the Singapore-MIT Alliance for Research and Technology (SMART) and National Science Foundation (NSF) grant CBET-1335938.

■ REFERENCES

(1) Raymer, D.; Smith, D. *Proc. Natl. Acad. Sci. U.S.A.* **2007**, *104*, 16432.
(2) Van Rensburg, E. J.; Sumners, D.; Wasserman, E.; Whittington, S. *J. Phys. A* **1992**, *25*, 6557.
(3) Virnau, P.; Kantor, Y.; Kardar, M. *J. Am. Chem. Soc.* **2005**, *127*, 15102−15106.
(4) Millett, K.; Dobay, A.; Stasiak, A. *Macromolecules* **2005**, *38*, 601−606.
(5) Wang, J. C. *Q. Rev. Biophys.* **1998**, *31*, 107−144.
(6) Staczek, P.; Higgins, N. P. *Mol. Microbiol.* **1998**, *29*, 1435−1448.
(7) Taylor, W. *Nature* **2000**, *406*, 916−919.
(8) Virnau, P.; Kardar, M.; Kantor, Y. *Chaos* **2005**, *15*, 41103−41103.
(9) Arsuaga, J.; Vázquez, M.; Trigueros, S.; Sumners, D. W.; Roca, J. *Proc. Natl. Acad. Sci. U.S.A.* **2002**, *99*, 5373−5377.
(10) Arsuaga, J.; Vazquez, M.; McGuirk, P.; Trigueros, S.; Sumners, D. W.; Roca, J. *Proc. Natl. Acad. Sci. U.S.A.* **2005**, *102*, 9165−9169.
(11) Sumners, D.; Whittington, S. *J. Phys. A* **1988**, *21*, 1689.
(12) Kardar, M. *Eur. Phys. J. B* **2008**, *64*, 519−523.
(13) Meluzzi, D.; Smith, D. E.; Arya, G. *Annu. Rev. Biophys.* **2010**, *39*, 349−366.
(14) Tubiana, L.; Rosa, A.; Fragiacomo, F.; Micheletti, C. *Macromolecules* **2013**, *46*, 3669−3678.
(15) Dai, L.; van der Maarel, J. R. C.; Doyle, P. S. *ACS Macro Lett.* **2012**, *1*, 732−736.
(16) Micheletti, C.; Orlandini, E. *Macromolecules* **2012**, *45*, 2113−2121.
(17) Micheletti, C.; Orlandini, E. *Soft Matter* **2012**, *8*, 10959−10968.
(18) Matthews, R.; Louis, A. A.; Likos, C. N. *ACS Macro Lett.* **2012**, *1*, 1352−1356.
(19) Poier, P.; Likos, C. N.; Matthews, R. *Macromolecules* **2014**, *47*, 3394−3400.
(20) Saitta, A. M.; Soper, P. D.; Wasserman, E.; Klein, M. L. *Nature* **1999**, *399*, 46−48.
(21) Arai, Y.; Yasuda, R.; Akashi, K.; Harada, Y.; Miyata, H.; Kinosita, K.; Itoh, H. *Nature* **1999**, *399*, 446−448.
(22) Kivotides, D.; Wilkin, S.; Theofanous, T. *Phys. Rev. E* **2009**, *80*, 041808.
(23) Rybenkov, V. V.; Cozzarelli, N. R.; Vologodskii, A. V. *Proc. Natl. Acad. Sci. U.S.A.* **1993**, *90*, 5307−5311.
(24) Matthews, R.; Louis, A. A.; Yeomans, J. M. *Phys. Rev. Lett.* **2009**, *102*, 088101.

(25) Rosa, A.; Di Ventra, M.; Micheletti, C. *Phys. Rev. Lett.* **2012**, *109*, 118301.
(26) Huang, L.; Makarov, D. E. *J. Chem. Phys.* **2008**, *129*, 121107.
(27) Metzler, R.; Reisner, W.; Riehn, R.; Austin, R.; Tegenfeldt, J.; Sokolov, I. *Europhys. Lett.* **2006**, *76*, 696.
(28) Tang, J.; Du, N.; Doyle, P. S. *Proc. Natl. Acad. Sci. U.S.A.* **2011**, *108*, 16153−16158.
(29) Renner, C. B.; Du, N.; Doyle, P. S. *Biomicrofluidics* **2014**, *8*, http://scitation.aip.org/content/aip/journal/bmf/8/3/10.1063/1.4878135 (accessed July 28, 2014).
(30) Hsieh, C.; Doyle, P. *Korea−Aust. Rheol. J.* **2008**, *20*, 127−142.
(31) Graham, M. D. *Annu. Rev. Fluid Mech.* **2011**, *43*, 273−298.
(32) Clarke, J.; Wu, H.-C.; Jayasinghe, L.; Patel, A.; Reid, S.; Bayley, H. *Nat. Nanotechnol.* **2009**, *4*, 265−270.
(33) Michaeli, Y.; Ebenstein, Y. *Nat. Biotechnol.* **2012**, *30*, 762−763.
(34) Bao, X.; Lee, H.; Quake, S. *Phys. Rev. Lett.* **2003**, *91*, 265506.
(35) Vologodskii, A. *Biophys. J.* **2006**, *90*, 1594−1597.
(36) Adams, C. *The knot book: an elementary introduction to the mathematical theory of knots*; AMS Bookstore, 2004.
(37) Jian, H.; Vologodskii, A. V.; Schlick, T. *J. Comput. Phys.* **1997**, *136*, 168−179.
(38) Klenin, K.; Merlitz, H.; Langowski, J. *Biophys. J.* **1998**, *74*, 780−788.
(39) Stigter, D. *J. Colloid Interface Sci.* **1975**, *53*, 296−306.
(40) Stigter, D. *Biopolymers* **1977**, *16*, 1435−1448.
(41) Huang, L.; Makarov, D. E. *J. Phys. Chem. A* **2007**, *111*, 10338−10344.
(42) Koseleff, P.-V.; Pecker, D. 2012, arXiv:1203.4376. arXiv.org e-Print archive. http://arxiv.org/pdf/1203.4376.pdf (accessed July 28, 2014).
(43) Matthews, R.; Louis, A.; Yeomans, J. *Europhys. Lett.* **2010**, *89*, 20001.
(44) Belmonte, A. In *Physical and Numerical Models in Knot Theory*; Calvo, J. A., Ed.; Series on Knots and Everything; World Scientific: River Edge, NJ, 2005; Vol. *36*.
(45) Marenduzzo, D.; Micheletti, C.; Orlandini, E.; Sumners, D. W. *Proc. Natl. Acad. Sci. U.S.A.* **2013**, *110*, 20081−20086.
(46) Di Stefano, M.; Tubiana, L.; Di Ventra, M.; Micheletti, C. *Soft Matter* **2014**, *10*, 6491−6498.
(47) Borujeni, E. E.; Zydney, A. L. *J. Membr. Sci.* **2014**, *450*, 189−196.